

Supporting Information

Near-field Spectral Mapping of Individual Exciton Complexes of Monolayer WS₂ Correlated with Local Defects and Charge Populations

Yongjun Lee,^{a,b} Seok Joon Yun,^{a,b} Youngbum Kim,^{a,b} Min Su Kim,^b Gang Hee Han,^b A. K.
Sood,^c and Jeongyong Kim^{*a,b}

^aCenter for Integrated Nanostructure Physics, Institute for Basic Science, Suwon 440-746, Republic of Korea

^bDepartment of Energy Science, Sungkyunkwan University, Suwon 440-746, Republic of Korea

^cDepartment of Physics, Indian Institute of Science, Bangalore-560012, India

*Email: j.kim@skku.edu

Figure S1. Schematic of the near-field PL set up.

Figure S2. Comparison AFM image vs near-field PL image.

Figure S3. Spatial profile of A⁰ and A⁻.

Figure S4. P-type doping effect by water adsorption.

Figure S5. How to make contrast enhanced image of X^D.

Figure S6. The location of X^D.

Figure S7. Exfoliated 1L-WS₂ near-field PL images and spectra.

Figure S8. Large area image of near-field PL image used in Figure 5 and categorized PL spectra by emission intensity.

Figure S9. Absorption spectrum and calculation of the density of photoexcited states.

Figure S10. PL images and PL spectra with different excitation laser power.

Figure S11. Strong PL emission near the line defects.

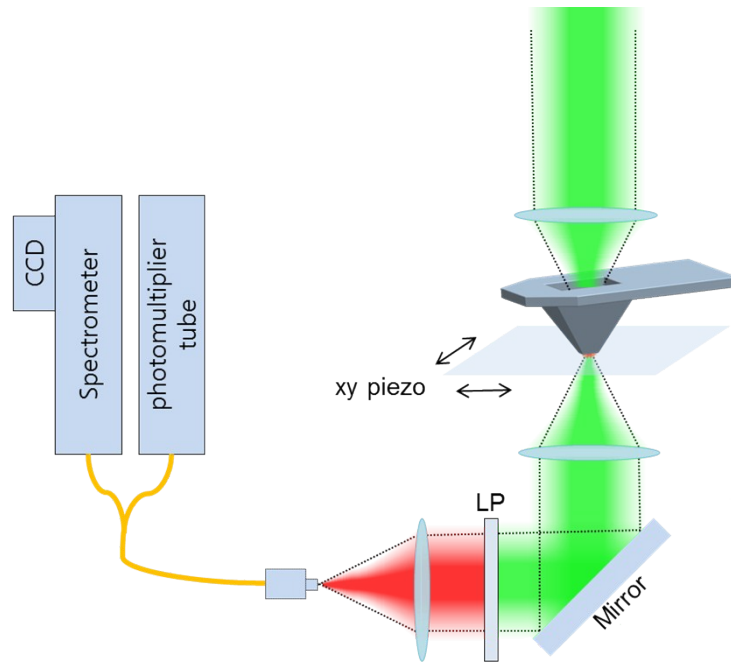


Figure S1. Schematic of the near-field PL imaging and spectroscopy set up. The transmission throughput of our near-field probe was estimated to be $\sim 1.4 \times 10^{-4}$, as detailed in a previous report.¹ Based on this value, we expected the input power values of 6 mW and 20 mW to have yielded laser power values on the sample of $\sim 0.8 \mu\text{W}$ ($1.0 \times 10^4 \text{ W/cm}^2$) and $2.8 \mu\text{W}$ ($3.6 \times 10^4 \text{ W/cm}^2$), respectively. (LP : longpass filter)

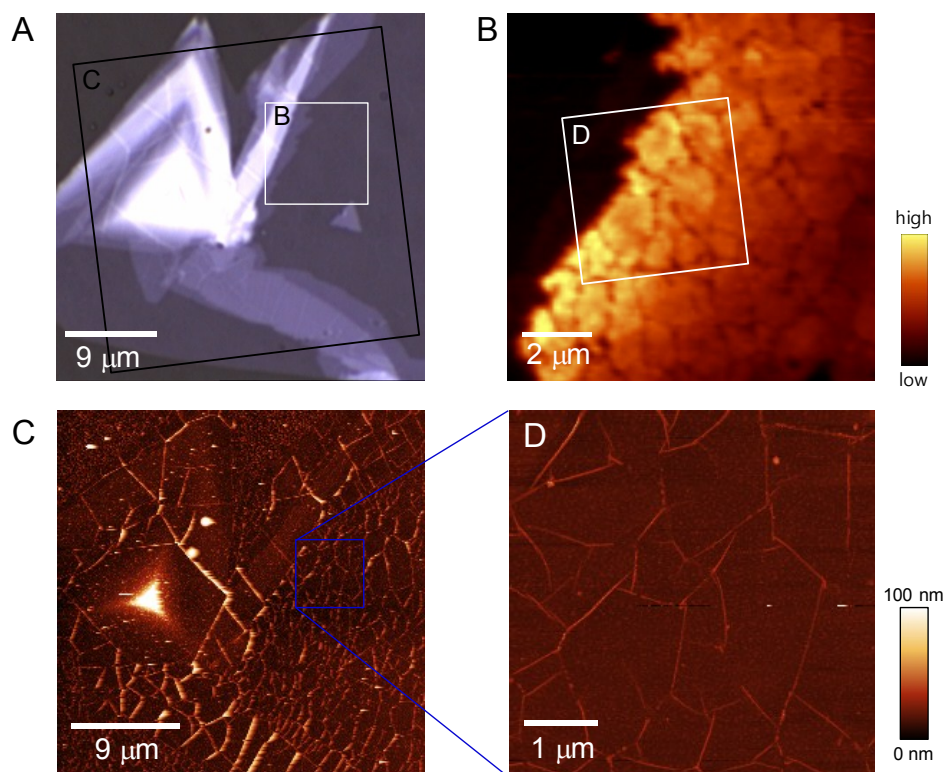


Figure S2. (A) Optical microscope image of CVD WS₂ flake. (B) Near-field PL emission image of white boxed region in A. (the range of 2.1 - 1.7 eV) (C) atomic force microscope topography image of selected area of black boxed region in A. (D) selected AFM image of blue boxed region in C and white boxed region in B.

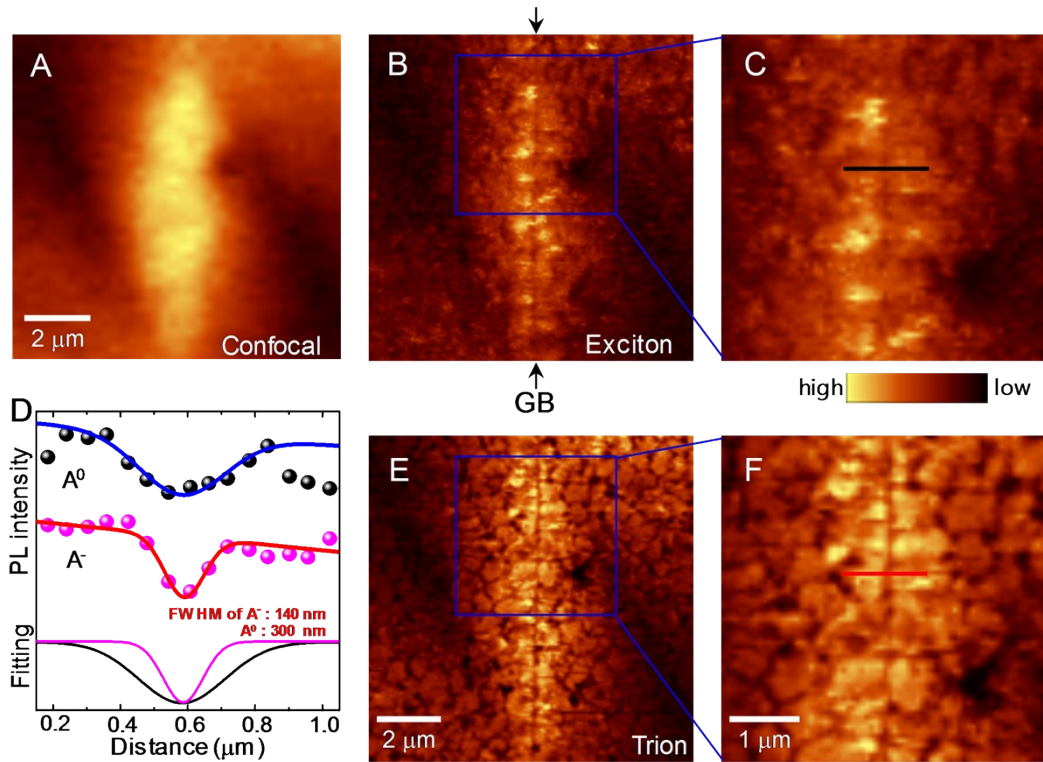


Figure S3. (A) Confocal PL image of 1L-WS₂ around a grain boundary. (B) and (E) Deconvoluted near-field PL emission images of neutral excitons (A^0) and trions (A^-) in the same area as (A), respectively. At the grain boundary (arrow), the emission intensities from both A^0 and A^- were reduced, but these emissions showed different spatial extents. (C) and (F) Expanded images of A^0 and A^- profiles of the boxed areas in B and E, respectively. (D) Representative line profiles of A^0 (black dot), A^- (pink dot) images with Gaussian fitting (A^0 : blue, A^- : red). Full width at half maximum (FWHM) of each Gaussian curve fit is indicated by red text. A^0 yielded an ~ 300 nm FWHM while A^- displayed an ~ 140 nm FWHM in line profiles across the grain boundary. This significant difference suggests the diffuse and localized natures of A^0 and A^- , respectively.

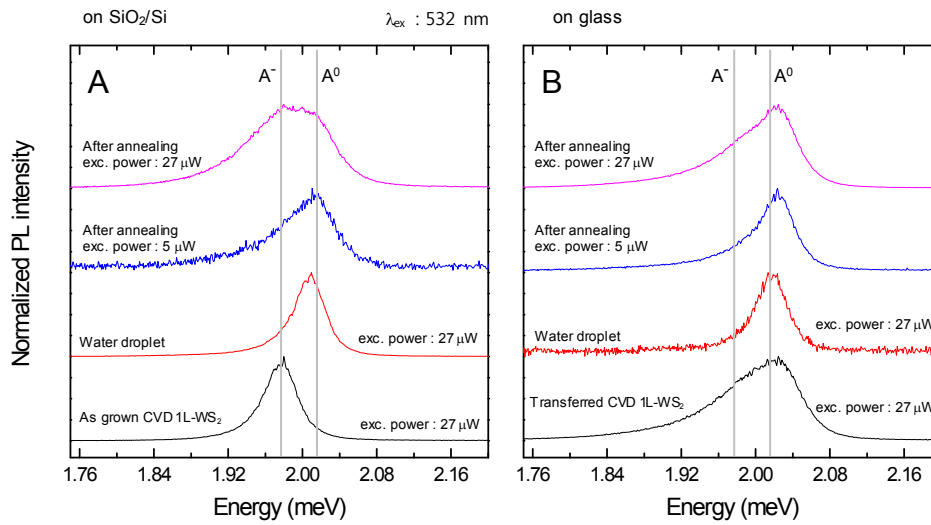


Figure S4. P-type doping effect by H₂O molecules adsorption. PL spectra of as grown CVD 1L-WS₂ on SiO₂/Si (A) or transferred CVD 1L-WS₂ on glass (B). Excitation wavelength : 532 nm.

Black : as grown 1L-WS₂, transferred 1L-WS₂ in air

Red : samples with water droplet and covered by a cover glass.

Blue : samples were annealed in air at temperature, 100 °C for 20 minutes. The excitation power was 5 μW.

Pink : same sample with blue, but the excitation power was 27 μW.

All measurements were taken under excitation power 27 μW, except blue line.

Gray lines are indicating exciton peak position (A⁰) and trion peak position (A⁻) for clarity.

The values of each peak position were averaged from the value used in Fig. 4C in main text.

The emission spectral weight of exciton was dominant after water droplet. After annealing, the emission spectral weight of exciton decreases due to the removal of the H₂O molecules.

Similar phenomena was reported which was also attributed to the H₂O molecules adsorption and removal.²

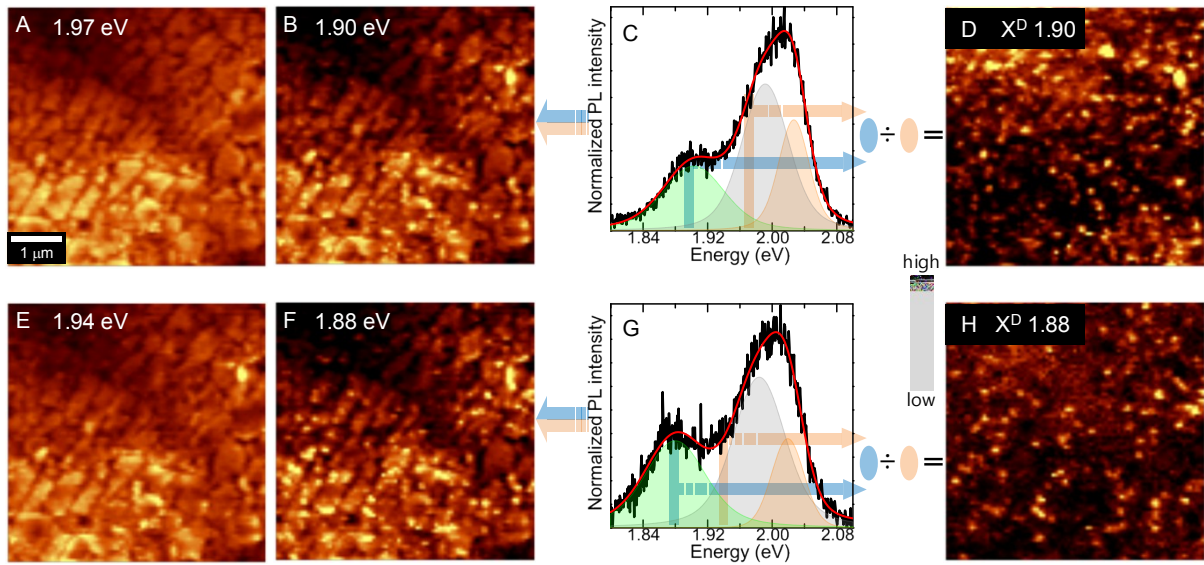


Figure S5. (A, B, E, F). Near-field PL images at energy levels of 1.97, 1.90, 1.94, and 1.88 \pm 0.002 eV, respectively. (C, G). Representative near-field PL spectra containing defect-bound localized exciton (X^D) peaks located at 1.90 eV and 1.88 eV, respectively. X^D contrast-enhanced PL images were obtained by dividing image B (or F) by A (or E) to yield D (or H), which displayed the higher contrasts for X^D s by having partially eliminated the background signals of trions strongly present in the PL images at X^D peak energies (B and F images) due to the spectral overlap between X^D peaks and trion peaks.

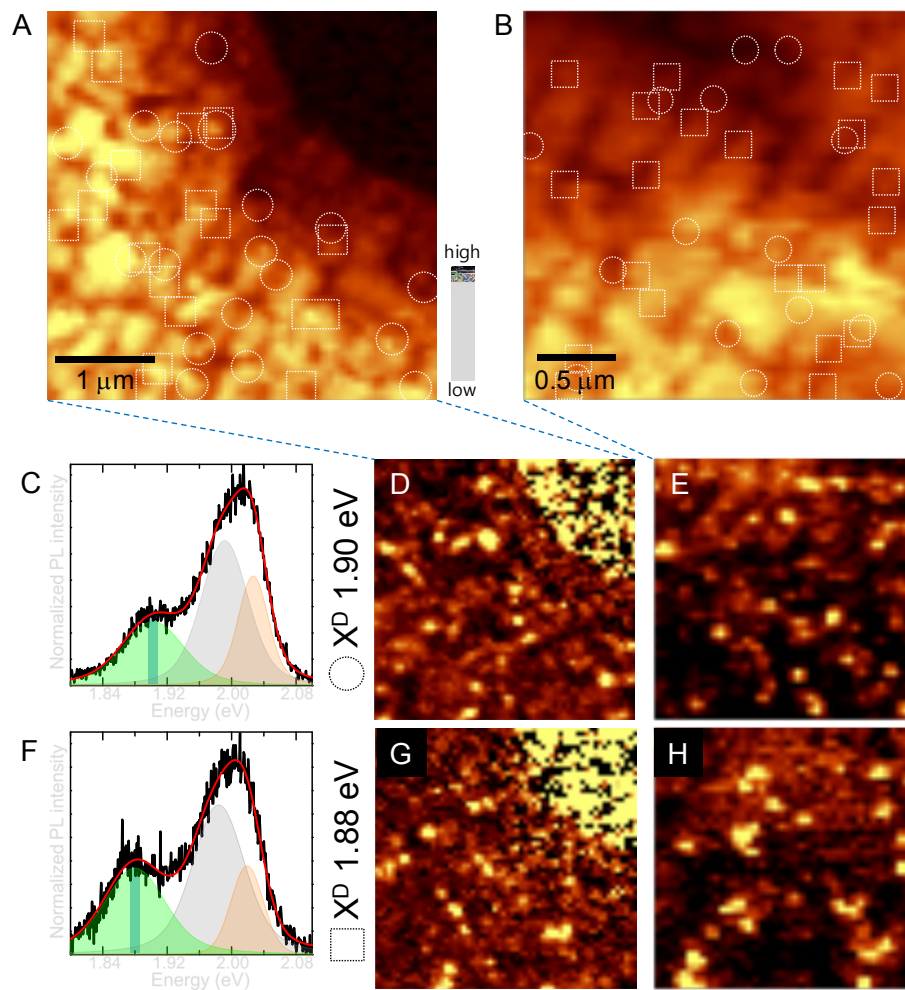


Figure S6. (A, B) Near-field PL images of the 1L-WS₂ edge and GB region (total integrated PL intensity). White dotted circles indicate the locations of X^Ds that appeared with an energy level of 1.90 eV, and squares are for 1.88 eV. (C, F) Representative PL spectra containing X^D peaks at 1.90 eV and 1.88 eV. (D, E) PL images processed as described in Supplemental Figure 3 for X^D emissions at 1.90 eV for the region shown in A and B, respectively. (G, H) PL images processed for X^D emissions at 1.88 eV for the regions shown in A and B, respectively. [Note the spatial correlation between locations of X^D excitons and the line defects.]

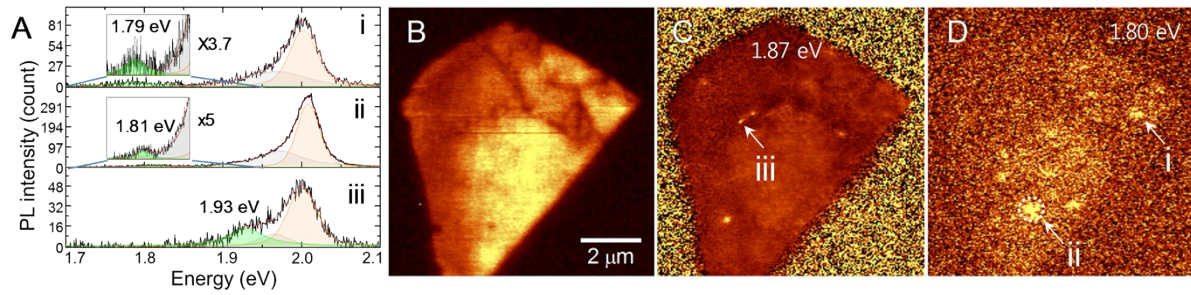


Figure S7. (A) Near-field PL spectra obtained from three selected locations (i, ii and iii) of C and D. Orange curve: A^0 peak, gray curve: A^- peak, green curve: X^D peak. Insets are magnified spectra at X^D peak positions. (B, C, D) Near-field PL images of exfoliated 1L-WS₂, (B) over the spectral range 1.7-2.1 eV, at (C) 1.87eV and at (D) 1.80eV, respectively. Contrast enhancement process (described in Fig. S5) was used for the image in (C).

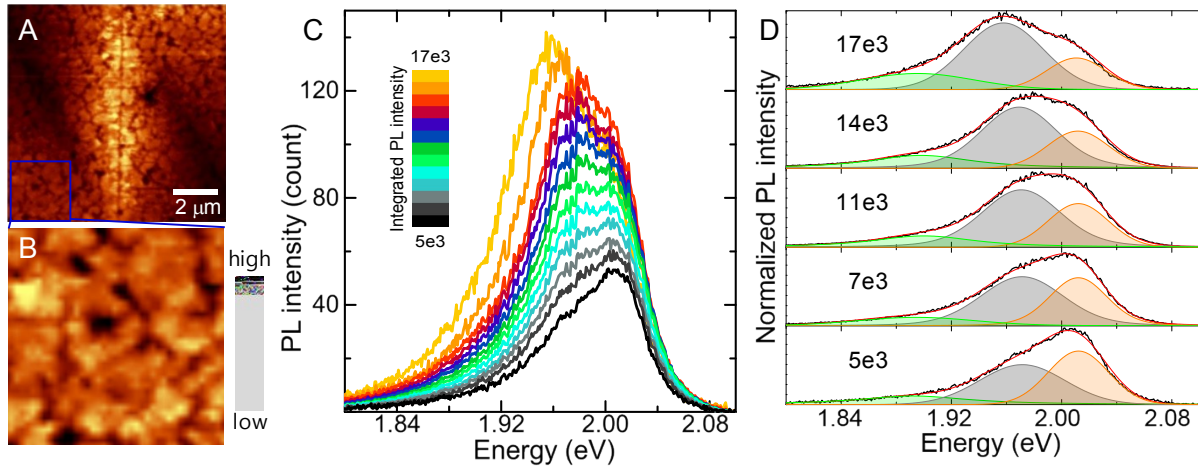


Figure S8. (A) Near-field PL image of a grain boundary region. (B) Magnified image of white boxed region in A. (C) PL spectra averaged from the pixels of the image in B (the same region as in Fig. 2A) corresponding to 13 PL intensity levels ranging from 5×10^3 to 17×10^3 . The PL intensity is in photon counts and the PL spectra are color-coded with the figure legend. Systematic redshift and broadening of PL curves resulted from the increasing spectral weight of A^- with increasing PL intensity. (D) Fitting results of PL spectra obtained from five selected points in Fig. 5. Orange, gray, green, red curves represent the fitting curves of A^0 , A^- , X^D and total sum of all curves, respectively.

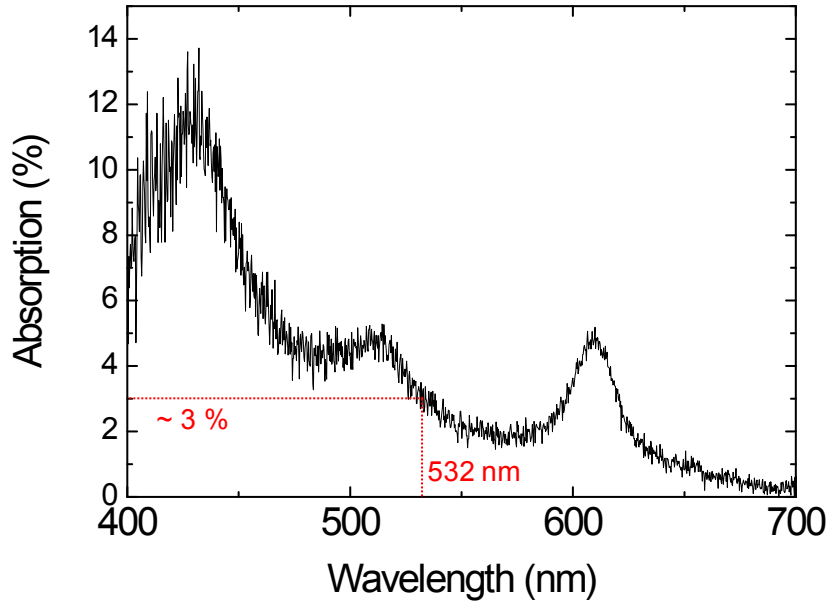


Figure S9. The absorption spectrum of 1L-WS₂. The absorption of 1L-WS₂ was ~3 % at 532 nm. This value was used for calculation of the density of photoexcited states.

The density of photoexcited states (N_{total}) is calculated using below equations.

$$N_{total} = N_{non} + N_{rad}$$

$$N_{non} = a(1 - Q)\left(\frac{I}{E}\right)t_{non}$$

$$N_{rad} = aQ\left(\frac{I}{E}\right)t_{rad}$$

Here, N_{non} and N_{rad} are numbers of non-radiative and radiative recombination, respectively.

a : absorption = 3 %

Q : quantum yield of 1L-WS₂ = 6 %.³

I : power density of laser excitation = 1.0×10^4 W/cm² for 6 mW and 3.6×10^4 cm⁻² for 20 mW laser input powers.

E : energy of laser light = 3.72×10^{-19} J

t : exciton recombination time = 13 ns for radiative recombination time (t_{rad}), and 900 ps for non-radiative recombination time (t_{non}).³

The calculated the density of photo-excited states are $1.34 \times 10^{12} \text{ cm}^{-2}$ and $4.67 \times 10^{12} \text{ cm}^{-2}$ for 6 mW and 20 mW laser excitation powers, respectively.

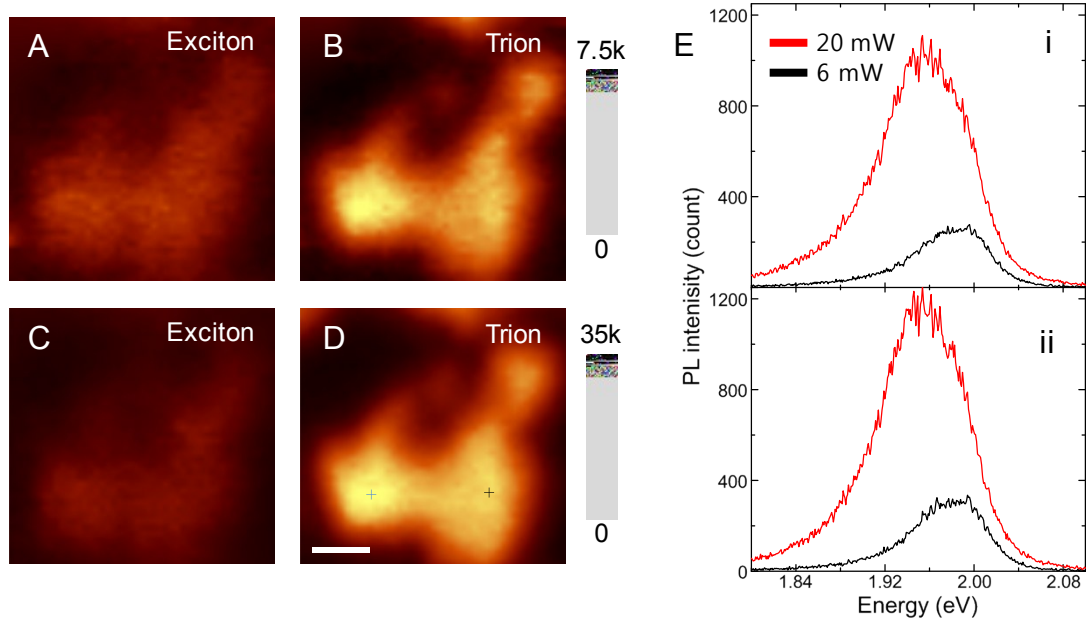


Figure S10. (A, B) PL images of A⁰ and A⁻ emissions at 6 mW input power. (C, D) PL images of A⁰ and A⁻ emissions at 20 mW input power. Scale bar: 200 nm. (E) near-field PL spectra of 1L-WS₂ at two selected locations (crosses in D). (Black : 6 mW, red: 20 mW).

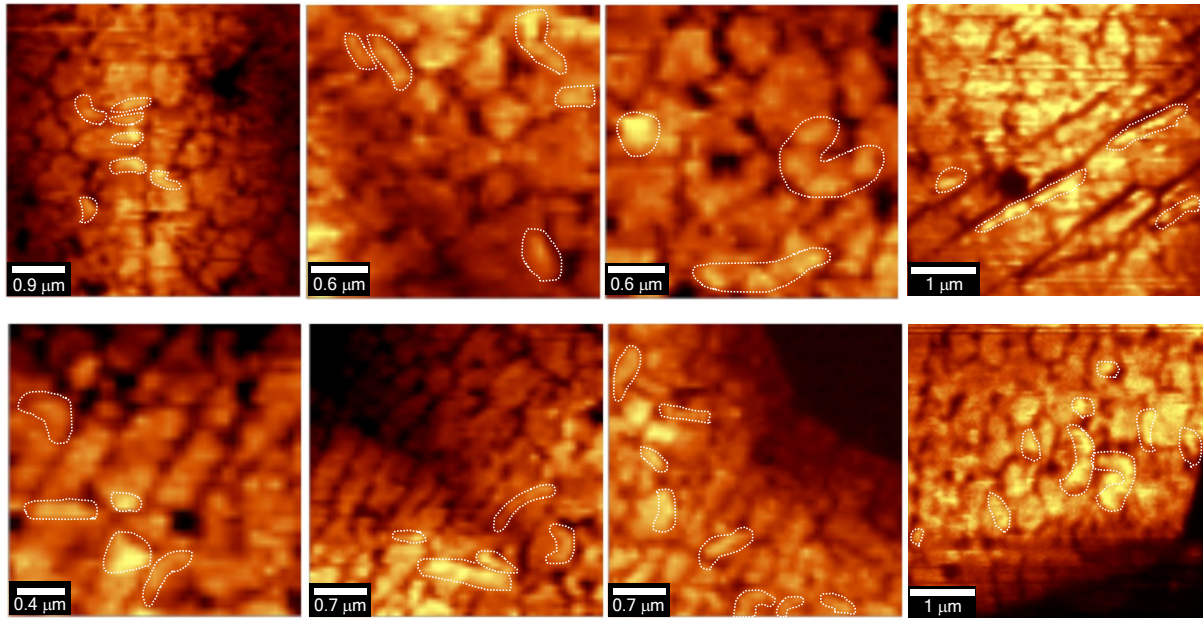


Figure S11. Strong PL emissions near the line defects

Reference

1. Y. Lee, S. Park, H. Kim, G. H. Han, Y. H. Lee and J. Kim, *Nanoscale*, 2015, **7**, 11909-11914.
2. N. Peimyoo, W. Yang, J. Shang, X. Shen, Y. Wang and T. Yu, *ACS Nano*, 2014, **8**, 11320-11329.
3. L. Yuan and L. Huang, *Nanoscale*, 2015, **7**, 7402-7408.